Probabilistic Engineering Mechanics 74 (2023) 103493

Contents lists available at ScienceDirect

Probabilistic Engineering Mechanics

journal homepage: www.elsevier.com/locate/probengmech

Extending the analysis of the Euler–Bernoulli model for a stochastic static cantilever beam: Theory and simulations

Juan-Carlos Cortés *, Elena López-Navarro, Pablo Martínez-Rodríguez, José-Vicente Romero, María-Dolores Roselló

Instituto Universitario de Matemática Multidisciplinar, Universitat Politècnica de València, Camíde Vera, s/n, València, 46022, Spain

ARTICLE INFO

Keywords:
Static cantilever beam
Probability density function
Principle of maximum entropy
Dirac delta function
Generalized functions
Random bending moment
Random shear force
Poisson probability distribution
Monte Carlo simulations

ABSTRACT

In this paper, we present a comprehensive probabilistic analysis of the deflection of a static cantilever beam based on Euler–Bernoulli's theory. For the sake of generality in our stochastic study, we assume that all model parameters (Young's modulus and the beam moment of inertia) are random variables with arbitrary probability densities, while the loads applied on the beam are described via a delta-correlated process. The probabilistic study is based on the calculation of the first probability density function of the solution and the probability density of other key quantities of interest, such as the shear force, and the bending moment, which are treated as random variables too. To conduct our study, we will first calculate the first moments of the solution, which is a stochastic process, and we then will take advantage of the Principle of Maximum Entropy. Furthermore, we will present an algorithm, based on Monte Carlo simulations, that allows us to simulate our analytical development computationally. The theoretical findings will be illustrated with numerical examples where different realistic probability distributions are assumed for each model random parameter.

1. Introduction

Beams are considered one of the most important structural elements in civil engineering. They are key elements to support the floor of a building, as structural components of bridges, or to build balconies, just to cite a few. If we apply loads to these above-mentioned beams, for example, the own weight of building materials or furniture, the flow of cars on a bridge, or people on the balcony, we have to ensure that the structure can support these loads so as not to collapse. To properly design a beam, it is necessary to know some key engineering characteristics, such as the static deflection, the bending moment, or the shear force. To mathematically describe these characteristics, as a first simplified approach, we can use Euler–Bernoulli's beam theory, also called shear rigid-beam or classical beam theory, [1]. Euler–Bernoulli's beam model is a simplification of the theory of elasticity that allows us to model the deflection of a static straight-axis beam as a function of the applied load, provided it undergoes small deflections. The deflection of a beam using Euler–Bernoulli's beam model has been widely studied from a deterministic point of view [2–4]. However, it is more realistic to approach the corresponding study from a stochastic standpoint since uncertainties are often present due to, for example, the heterogeneity of the beam materials or the lack of knowledge of the physical phenomenon because of its own inherent complexity. More accurately, the heterogeneity of the beam materials makes it more realistic to assume that both the values of the beam's moment of inertia and Young's modulus are random variables rather than deterministic constants. In addition, the loads applied on a beam may vary randomly at each of its spatial points due to environmental factors (such as the wind pressure or the snow load on the ground) or to the use for which it has been built (such as the flow of people on balconies, or vehicles on bridges), for instance. This latter motivates modeling the load on a beam by a spatial stochastic process rather than via a deterministic function. These reasons have motivated numerous probability-based methods over the last few decades to better design and analyze civil engineering structures. For instance, in [5], it is obtained the mean and covariance of the deflection of a simply supported beam with stochastic bending flexibility, assuming that the load is deterministic. In [6], authors assume that elastic modulus is a random variable, then the stochastic finite element method is applied to calculate the mean, standard deviation, and coefficient of displacements. In [7], the authors combine polynomial chaos with Neumann expansion method to obtain closed-form expressions for the first two response moments and, then they apply the results to a cantilever beam, where the bending rigidity of the beam is assumed to be a stationary Gaussian random field.

In this paper, we perform a full probabilistic study of the deflection of a static cantilever beam using the Euler–Bernoulli's model with main novelty that all its parameters (Young's modulus and the beam moment of inertia) are treated as random variables and that the load applied

* Corresponding author.
E-mail address: jccortes@imm.upv.es (J.-C. Cortés).

https://doi.org/10.1016/j.probengmech.2023.103493
Received 28 April 2023; Received in revised form 15 June 2023; Accepted 17 July 2023
Available online 22 July 2023

on the beam is assumed to be described by a delta-correlated process. We will calculate the solution's first probability density function (1-PDF) via the Principle of Maximum Entropy (PME). To achieve this goal, we first calculate the first statistical moments of the solution. To complete the study, we also determine the PDF of the shear force, and the bending moment, which are treated as random variables. We also introduce an algorithm, based on Monte Carlo method, to carry out simulations from our theoretical findings. It is important to point out that the calculation of the first moments of the solution is based on the so-called generalized functions. This technique is introduced in [8], where authors elegantly analyze other types of beams, different from a cantilever, assuming partial randomization of the models under study. Particularly, they assume the flexural rigidity parameter is deterministic. In the present paper, apart from studying another type of beam, namely the cantilever, dealing with the full randomization of the corresponding Euler–Bernoulli's model, we also obtain the 1-PDF of the solution, which is the most important information associated with a stochastic process since from the 1-PDF one can determine any one-dimensional statistical moment as well as the probability that the deflection varies on a specific interval of interest. This is key information to, for example, analyze and quantify the main risks that may affect civil structures.

The paper is organized as follows. Section 2 introduces some deterministic and stochastic preliminaries required to conduct the probabilistic study of the deflection of a cantilever beam subject to loads spanned according to a delta-correlated process with random pulse intensities (representing the loads) and assuming that the model parameters, namely, the material Young's modulus of elasticity and the beam moment of inertia are random variables. In Section 3, we carry out the analysis of the stochastic model by first computing, under very general conditions, the mean and variance of the deflection. With the goal of approximating later its 1-PDF taking advantage of the PME method. Apart from the deflection, we also calculate approximations of mean, the variance, and the PDF of other relevant physical quantities associated to the beam as the bending moment and the shear force. In Section 4, we present an algorithm, based on Monte Carlo simulations, that allows us to simulate all the abovementioned physical quantities effectively. The theoretical results obtained in Section 3 are compared with the ones obtained via simulations using the algorithm presented in Section 4. Finally, conclusions are drawn in Section 6.

2. Problem setting and preliminaries

For the sake of completeness, this section is addressed to introduce the model equations and some technical deterministic and stochastic results that will be required throughout the paper.

2.1. Equations governing the problem and physical interpretation

It is well-known that the following linear fourth-order differential equation governs the static deflection of a beam of length l [9, Chapter 12],

$$\frac{\mathrm{d}^4 Y(x)}{\mathrm{d}x^4} = \frac{1}{EI} Q(x), \quad 0 < x < l, \tag{1}$$

where $Y(x)$ represents the deflection curve, E is the material's Young's modulus of elasticity, I is the beam moment of inertia about the neutral axis, and the product EI is known as the flexural stiffness. $Q(x)$ represents the distribution of the downward force acting vertically on the beam at each spatial point $x \in (0, l)$.

The above differential equation describes the beam deflection for each load case and support configuration, such as embedded at both ends, embedded and supported, with a free end, etc. In our setting, we will consider a cantilever beam, i.e., a beam embedded on the left side ($x = 0$) and free on the right side ($x = l$). The boundary conditions corresponding to this case are then given by

$$\begin{aligned} &Y(0) = 0, \quad \text{(null deflection in the embedment)},\\ &Y'(0) = 0, \quad \text{(null slope in the embedment)},\\ &Y''(l) = 0, \quad \text{(null moment in the free end)},\\ &Y'''(l) = 0, \quad \text{(null shear in the free end)}. \end{aligned} \tag{2}$$

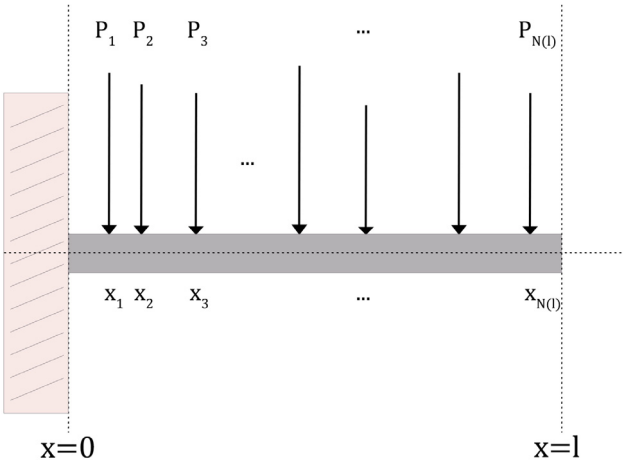

Fig. 1. Graphical representation of model (1), where the distribution of the random concentrated loads, P_i, on the spatial points x_i of the beam is described by the stochastic process given in (3).

Based on the reasons explained in Section 1, we will consider that the distribution of the load supported on the beam, $Q(x)$, is described by a stochastic process. Specifically, we will assume that $Q(x)$ is determined by concentrated loads, P_i, acting vertically on the beam and randomly spanned according to the following expression,

$$Q(x) = \sum_{i=1}^{N(l)} P_i R_{-1}(x - x_i), \tag{3}$$

where P_i are assumed to be independent and identically distributed (i.i.d.) random variables, representing concentrated loads acting at the abscissas $x_i \in (0, l)$. $N(l)$ denotes a Poisson counting process with rate $\lambda > 0$. This parameter can be interpreted as the expected number of random loads, P_i, that randomly apply per unit of space on the beam. Following the notation used in [10], we use the term $R_{-1}(x - x_i) := \delta(x - x_i)$ to indicate that P_i, $1 \le i \le n$, represent concentrated loads at the spatial points x_i. Here, $\delta(\cdot)$ denotes the Dirac delta function. Furthermore, hereinafter we will assume that E and I are independent random variables, so notice that they do not depend on x. Fig. 1 shows a graphical representation of the model.

Notice that elements having different natures appear in the model formulation. Indeed, while $R_{-1}(\cdot)$, l and λ are deterministic, $N(l)$, P_i, E and I are stochastic. For the sake of completeness, in the following subsections, we will describe some relevant ingredients that will be required throughout the paper.

2.2. Deterministic ingredients

As it has been used in the previous subsection, we will use the most well-known generalized function in $Q(x)$, i.e., the Dirac delta function. We will use this function to represent a concentrated load at an arbitrary spatial point, say x_0. Defining

$$R_{-1}(x - x_0) := \delta(x - x_0), \tag{4}$$

by integration, we obtain $R_0(x - x_0)$, which is the unit step or Heaviside function. If we continue integrating up to order $n \in \mathbb{N}$, we arrive at the

following piecewise polynomial function

$$R_n(x-x_0)=\begin{cases}0, & \text{if } x<x_0,\\ \frac{1}{n!}(x-x_0)^n, & \text{if } x\geq x_0,\end{cases} \tag{5}$$

that, for $n=1,2,3$, corresponds to the linear, quadratic, and cubic ramp functions, respectively. Notice that, (5) also works for $n=0$. As it shall be seen later, these functions $R_0(\cdot)$, $R_1(\cdot)$, $R_2(\cdot)$ and $R_3(\cdot)$ will be extensively used in our subsequent calculations.

2.3. Stochastic ingredients

The stochastic process given by (3) is known as the delta-correlated process [11] (also termed Poisson white noise process [12, p. 186]). The process $Q(x)$ can be regarded as the formal derivative of its corresponding associated compound Poisson process, $C(x)=\sum_{i=1}^{N(l)}P_i$, $0<x<l$, i.e. $\frac{\mathrm{d}C(x)}{\mathrm{d}x}=Q(x)$. As we have seen before, this process consists of a Poisson counting process, $N(l)$, and random intensities, P_i, acting at the spatial points on the beam, x_i, $i=1,\dots,N(l)$ (this action is mathematically represented by $P_iR_{-1}(x-x_i)$). The loads P_i are distributed along the beam according to a Poisson distribution. This process is widely used to model concentrated loads simulating, for example, cars traveling on a bridge, which has motivated its consideration in our analysis.

We now introduce several statistical properties that will play a key role later for a class of random processes that include, as a particular case, the foregoing random processes $Q(x)$ and

$$G_j(x):=\sum_{i=1}^{N(l)}P_iR_j(x-x_i),\quad j=0,\dots,3, \tag{6}$$

are filtered Poisson processes [13], which depend on the loads, P_i, which are randomly spanned on the beam according to a Poisson counting process $N(l)$.

closely related to it that will be introduced later (see (6)). Let

$$Z(x)=\sum_{i=1}^{N(l)}U_iv(x,x_i) \tag{7}$$

be a stochastic process constructed by superposition of pulses at the spatial points x_i whose shape is defined by a deterministic function $v=v(x,x_i)$ and having pulse intensities given by a family of independent and identically distributed (i.i.d.) random variables U_i. As shown in [13], the probabilistic structure of $Z=Z(x)$ can be revealed via the characteristic functional. Indeed, it can be shown that the cumulant function of order m of Z is given by

$$C_Z^{(m)}(x_1,\dots,x_m)=\lambda\mathbb{E}\left[U^m\right]\int_0^{\min(x_1,\dots,x_m)}v(\rho,x_1)\cdots v(\rho,x_m)d\rho. \tag{8}$$

Note that we here have used $x_1,\dots,x_m$ to denote the variables of function C_Z for the sake of consistency with the independent variable x of Z, although any other letter could be used too. As a consequence of the properties of cumulants [13], the mean and the covariance can be obtained as particular cases of $C_{Z(x)}^{(m)}(x_1,\dots,x_m)$:

$$\mu_Z(x)=\mathbb{E}\left[Z(x)\right]=\lambda\mathbb{E}\left[U\right]\int_0^x v(\rho,x)d\rho=C_{Z(x)}^{(1)}(x), \tag{9}$$

and

$$\begin{aligned}\mathbb{C}\mathrm{ov}_Z(x_1,x_2)&=\mathbb{E}\left[Z(x_1)Z(x_2)\right]-\mathbb{E}\left[Z(x_1)\right]\mathbb{E}\left[Z(x_2)\right]\\&=\lambda\mathbb{E}\left[U^2\right]\int_0^{\min(x_1,x_2)}v(\rho,x_1)v(\rho,x_2)d\rho\\&=C_Z^{(2)}(x_1,x_2).\end{aligned} \tag{10}$$

Hence, the variance is given by

$$\sigma_Z^2(x)=C_Z^{(2)}(x,x). \tag{11}$$

Later we will also need to handle the cross-covariance of two stochastic processes, say $Z_v=Z_v(x)$ and $Z_w=Z_w(x)$, of the form of (7) with different shapes, v and w,

$$Z_v(x)=\sum_{i=1}^{N(l)}U_iv(x,x_i),\quad Z_w(x)=\sum_{i=1}^{N(l)}U_iw(x,x_i). \tag{12}$$

In this case, the cross-cumulant function of order $m=2$, which is just the cross-covariance of Z_v and Z_w, writes

$$C_{Z_v,Z_w}^{(2)}(x_1,x_2)=\lambda\mathbb{E}\left[U^2\right]\int_0^{\min(x_1,x_2)}v(\rho,x_1)w(\rho,x_2)d\rho. \tag{13}$$

As it shall be seen in the next section, these properties will be essential to obtain, in the first step, the mean and the variance of $Y(x)$, i.e., the deflection of the cantilever beam. Afterward, from these two statistics, we will approximate the 1-PDF of the solution taking advantage of the PME. Here, we point out that the computation of the 1-PDF is a key piece of information since, from its integration, one can calculate any one-dimensional statistical moments,

$$\mathbb{E}[Y(x)^m]=\int_{-\infty}^{\infty}y^mf_{Y(x)}(y)dy,\quad m=1,2,\dots \tag{14}$$

provided they exist. Furthermore, the 1-PDF permits computing the probability that the solution varies within a specific interval of interest,

$$\mathbb{P}[y_1\leq Y(x)\leq y_2]=\int_{y_1}^{y_2}f_{Y(x)}(y)dy,\quad 0<x<l. \tag{15}$$

Furthermore, we will determine other engineering probabilistic quantities of interest associated with the beam, such as the bending moment and the shear force.

As shown in [14], for fixed $x\in(0,l)$, the PME is an efficient method to obtain the PDF, $f_{Y(x)}:=f_{Y(x)}(y)$, of the random variable $Y(x)$, using the statistical information available, such that its support, moments, etc. Assuming that $Y(x)$ is an absolutely continuous random variable with support $\mathcal{D}(Y(x))$ and that its first two moments are known, then the PME seeks an approximation of the PDF of $Y(x)$ that maximizes the Shannon's entropy

$$S(f_{Y(x)})=\mathbb{E}\left[-\ln(f_{Y(x)}(Y(x)))\right]=-\int_{\mathcal{D}(Y(x))}f_{Y(x)}(y)\ln(f_{Y(x)}(y))dy, \tag{16}$$

subject to the constraints

$$\int_{\mathcal{D}(Y(x))}f_{Y(x)}(y)dy=1,\quad \int_{\mathcal{D}(Y(x))}y^nf_{Y(x)}(y)dy=\mathbb{E}[Y^n(x)],\ n=1,2. \tag{17}$$

Note that the PME utilizes the information of the moments of $Y(x)$ (in our setting representing the deflection of the beam at the spatial point x). As we shall first calculate the mean and the variance (or equivalently the second order moment) of $Y(x)$, we will take advantage of the PME to approximate the PDF of $Y(x)$.

Using the variational formulation of the method of Lagrange multipliers, it can be seen that the PDF of $Y(x)$ has the following form

$$f_{Y(x)}(y)=\mathbb{1}_{\mathcal{D}(Y(x))}e^{-1-\lambda_0-\lambda_1y-\lambda_2y^2}, \tag{18}$$

where $\mathbb{1}_{\mathcal{D}(Y(x))}$ is the characteristic function on the domain $\mathcal{D}(Y(x))$, and parameters λ_0,λ_1 and λ_2 can be calculated using the constraints defined in (17). Note that $\lambda_i=\lambda_i(x)$, $i=0,1,2$, depend on x, although it is omitted for convenience.

It is instructive to point out that the PME method has been widely applied in civil engineering. In [15], the authors obtain the PDF of the shear capacity of the reinforced concrete beam using PME and compare it with brute force Monte Carlo simulation, obtaining good approximations. In [16], the PME is modified to estimate the PDF of the material's fiber-reinforced concrete properties using their different order moments. In [17], authors combine polynomial chaos expansions with a variation of the classical PME to approximate the PDF of the response to several structural engineering problems. In [18], one proposes a new method for constructing the so-called probability box

(p-box) model based on the PME. The results are applied to perform a reliability analysis for uncertain engineering structures.

We finish this subsection devoted to the stochastic ingredients that will be required throughout this paper, indicating that, in the numerical simulations that will be shown in Section 5, we will apply Monte Carlo simulations. The Monte Carlo method is a popular, intuitive, and flexible approach to uncertainty quantification in virtually any class of mathematical problems whose data is affected by randomness. It is based on performing simulations of the random data according to their corresponding associated probabilistic laws. So, the method heavily relies on good random number generators. In its crude form, the error convergence rate is inversely proportional to the square root of the number of realizations of the random inputs. The Monte Carlo has been demonstrated to be a powerful tool to deal with stochastic/random engineering problems [19,20].

3. Concentrated loads P_i spanned randomly on the beam

In this section, we will carry out a probabilistic study of model (1). For the sake of clarity, we substitute expression (3) into Eq. (1) and we then obtain

$$\begin{cases} \dfrac{\mathrm{d}^4Y(x)}{\mathrm{d}x^4} = \dfrac{1}{EI}\displaystyle\sum_{i=1}^{N(l)} P_i R_{-1}(x-x_i), \quad 0<x<l, \\ Y(0)=0,\ \ Y'(0)=0,\ \ Y''(l)=0,\ \ Y'''(l)=0. \end{cases} \tag{19}$$

Integrating four times the model (19) and using the properties of R_{-1} and R_n, $n=0,1,2,3$, given in (4) and (5), respectively, it is easy to check that the stochastic solution is given by (see Appendix, for further details)

$$Y(x) = \frac{1}{EI}\left(G_3(x) - \frac{1}{6}G_0(l)x^3 - \frac{1}{2}\left(G_1(l) - lG_0(l)\right)x^2\right), \tag{20}$$

where $G_j(x)$ has been defined in (6).

The function $G_j(x)$ represents the load function, which is independent of the beam characteristics. However, for the sake of convenience in our subsequent computations, we introduce the following relabeling of the previous stochastic process $G_j(x)$,

$$\widehat{G}_j(x) = \sum_{i=1}^{N(l)} F_i R_j(x-x_i), \quad j=0,1,2,3, \qquad F_i = \frac{P_i}{EI}, \tag{21}$$

where $\widehat{G}_j(x)$ is now also dependent on the beam characteristics. This allows us to rewrite $Y(x)$ given in (20) in terms of the stochastic processes $\widehat{G}_j(x)$:

$$Y(x) = \widehat{G}_3(x) - \frac{1}{6}\widehat{G}_0(l)x^3 - \frac{1}{2}\left(\widehat{G}_1(l) - l\widehat{G}_0(l)\right)x^2. \tag{22}$$

As has been indicated in Section 2, we are interested in approximating the 1-PDF of the deflection of the beam, and for this goal, we shall apply the PME method. So we will first calculate the mean of the deflection, taking the expectation operator in expression (20)

$$\mathbb{E}[Y(x)] = \mathbb{E}[\widehat{G}_3(x)] - \frac{1}{6}\mathbb{E}[\widehat{G}_0(l)]x^3 - \frac{1}{2}\left(\mathbb{E}[\widehat{G}_1(l)] - l\mathbb{E}[\widehat{G}_0(l)]\right)x^2. \tag{23}$$

In order to provide an explicit representation of $\mathbb{E}[Y(x)]$, we shall compute $\mathbb{E}[\widehat{G}_j(x)]$, $j=0,\dots,3$. Notice that $\mathbb{E}[\widehat{G}_2(x)]$ is not specifically required for computing $\mathbb{E}[Y(x)]$, but it will be also calculated because will be needed later. To this end, we will take advantage of expectation $\mathbb{E}[Z(x)]$, given in (9), of the stochastic process $Z(x)$ defined in (7) with the following identification in terms of $\widehat{G}_j(x)$ defined in (21): the impulse shapes and pulse intensities are given by $v(x,x_i) := R_j(x-x_i)$, $j=0,\dots,3$, and $U_i := F_i$, respectively. Then, taking into account the definition of functions $R_j(x-x_j)$, given in (5), one obtains:

$$\begin{aligned} \mathbb{E}[\widehat{G}_0(x)] = C^{(1)}_{\widehat{G}_0}(x) &= \lambda\mathbb{E}\left[F_i\right]\int_0^x R_0(x-\rho)d\rho \\ &= \lambda\mathbb{E}\left[F_i\right]\int_0^x d\rho = \lambda\mathbb{E}\left[F_i\right]x, \end{aligned} \tag{24}$$

$$\begin{aligned} \mathbb{E}[\widehat{G}_1(x)] = C^{(1)}_{\widehat{G}_1}(x) &= \lambda\mathbb{E}\left[F_i\right]\int_0^x R_1(x-\rho)d\rho \\ &= \lambda\mathbb{E}\left[F_i\right]\int_0^x (x-\rho)d\rho = \frac{\lambda}{2}\mathbb{E}\left[F_i\right]x^2, \end{aligned} \tag{25}$$

$$\begin{aligned} \mathbb{E}[\widehat{G}_2(x)] = C^{(1)}_{\widehat{G}_2}(x) &= \lambda\mathbb{E}\left[F_i\right]\int_0^x R_2(x-\rho)d\rho \\ &= \lambda\mathbb{E}\left[F_i\right]\int_0^x \frac{1}{2}(x-\rho)^2d\rho = \frac{\lambda}{6}\mathbb{E}\left[F_i\right]x^3, \end{aligned} \tag{26}$$

and

$$\begin{aligned} \mathbb{E}[\widehat{G}_3(x)] = C^{(1)}_{\widehat{G}_3}(x) &= \lambda\mathbb{E}\left[F_i\right]\int_0^x R_3(x-\rho)d\rho \\ &= \lambda\mathbb{E}\left[F_i\right]\int_0^x \frac{1}{6}(x-\rho)^3d\rho = \frac{\lambda}{24}\mathbb{E}\left[F_i\right]x^4. \end{aligned} \tag{27}$$

Then, substituting the above expressions in (23), one gets the following expression for the expectation of $Y(x)$:

$$\mathbb{E}[Y(x)] = \frac{\lambda}{2}\mathbb{E}\left[F_i\right]\left(\frac{1}{12}x^4 - \frac{1}{3}lx^3 + \frac{1}{2}l^2x^2\right). \tag{28}$$

Now, we compute the covariance of $Y(x)$ using the representation (20) and its properties as a positive semidefinite function:

$$\begin{aligned} \mathbb{C}\mathrm{ov}_Y(x_1,x_2) &= \mathbb{E}\left[Y(x_1)Y(x_2)\right] - \mathbb{E}\left[Y(x_1)\right]\mathbb{E}\left[Y(x_2)\right] \\ &= C^{(2)}_{\widehat{G}_3}(x_1,x_2) - \frac{1}{2}C^{(2)}_{\widehat{G}_3\widehat{G}_1}(x_1,l)x_2^2 - \frac{1}{2}C^{(2)}_{\widehat{G}_3\widehat{G}_1}(x_2,l)x_1^2 \\ &\quad + \frac{1}{4}C^{(2)}_{\widehat{G}_1}(l,l)x_1^2x_2^2 + \frac{1}{2}C^{(2)}_{\widehat{G}_3\widehat{G}_0}(x_1,l)\left(lx_2^2 - \frac{1}{3}x_2^3\right) \\ &\quad + \frac{1}{2}C^{(2)}_{\widehat{G}_3\widehat{G}_0}(x_2,l)\left(lx_1^2 - \frac{1}{3}x_1^3\right) \\ &\quad + \frac{1}{4}C^{(2)}_{\widehat{G}_0}(l,l)\left(\frac{1}{9}x_1^3x_2^3 - \frac{l}{3}x_1^3x_2^2 - \frac{l}{3}x_1^2x_2^3 + l^2x_1^2x_2^2\right) \\ &\quad + \frac{1}{2}C^{(2)}_{\widehat{G}_0\widehat{G}_1}(l,l)\left(\frac{1}{6}x_1^3x_2^2 + \frac{1}{6}x_1^2x_2^3 - lx_1^2x_2^2\right). \end{aligned} \tag{29}$$

Taking $x_1=x_2=x$ in the above expression, using that $C^{(2)}_{\widehat{G}_j}(x,x) = \sigma^2_{\widehat{G}_j}(x)$, and after some algebraic manipulations, one can obtain the variance of $Y(x)$,

$$\begin{aligned} \sigma^2_Y(x) = C^{(2)}_Y(x,x) &= \mathbb{E}\left[Y(x)^2\right] - \mathbb{E}\left[Y(x)\right]^2 \\ &= \sigma^2_{\widehat{G}_3}(x) - C^{(2)}_{\widehat{G}_3\widehat{G}_1}(x,l)x^2 + \frac{1}{4}\sigma^2_{\widehat{G}_1}(l)x^4 + C^{(2)}_{\widehat{G}_3\widehat{G}_0}(x,l)\left(lx^2 - \frac{1}{3}x^3\right) \\ &\quad + \frac{1}{4}\sigma^2_{\widehat{G}_0}(l)\left(\frac{1}{9}x^6 - \frac{2}{3}lx^5 + l^2x^4\right) + \frac{1}{2}C^{(2)}_{\widehat{G}_0\widehat{G}_1}(l,l)\left(\frac{1}{3}x^5 - lx^4\right). \end{aligned} \tag{30}$$

In this expression, we now compute the terms of the form $\sigma^2_{\widehat{G}_j}$ and $C^{(2)}_{\widehat{G}_i\widehat{G}_j}$, using (11) and (13), respectively,

$$\sigma^2_{\widehat{G}_3}(x) = \lambda\mathbb{E}[F_i^2]\int_0^x R_3(x-\rho)R_3(x-\rho)d\rho = \frac{\lambda}{252}\mathbb{E}\left[F_i^2\right]x^7, \tag{31}$$

$$C^{(2)}_{\widehat{G}_3\widehat{G}_1}(x,l) = \lambda\mathbb{E}[F_i^2]\int_0^x R_3(x-\rho)R_1(l-\rho)d\rho = \frac{\lambda}{24}\mathbb{E}\left[F_i^2\right]x^4\left(l - \frac{1}{5}x\right), \tag{32}$$

$$\sigma^2_{\widehat{G}_1}(l) = \lambda\mathbb{E}[F_i^2]\int_0^l R_1(l-\rho)R_1(l-\rho)d\rho = \frac{\lambda}{3}\mathbb{E}\left[F_i^2\right]l^3, \tag{33}$$

$$C^{(2)}_{\widehat{G}_3\widehat{G}_0}(x,l) = \lambda\mathbb{E}[F_i^2]\int_0^x R_3(x-\rho)R_0(l-\rho)d\rho = \frac{\lambda}{24}\mathbb{E}\left[F_i^2\right]x^4, \tag{34}$$

$$\sigma^2_{\widehat{G}_0}(l) = \lambda\mathbb{E}[F_i^2]\int_0^l R_0(l-\rho)R_0(l-\rho)d\rho = \lambda\mathbb{E}\left[F_i^2\right]l, \tag{35}$$

$$C^{(2)}_{\widehat{G}_0\widehat{G}_1}(l,l) = \lambda\mathbb{E}[F_i^2]\int_0^l R_0(l-\rho)R_1(l-\rho)d\rho = \frac{\lambda}{2}\mathbb{E}\left[F_i^2\right]l^2. \tag{36}$$

Substituting these expressions into (30) and after simplifying, one gets the following expression of the variance

$$\sigma^2_Y(x) = \frac{\lambda}{12}\mathbb{E}[F_i^2]\left(-\frac{2}{105}x^7 + \frac{1}{3}lx^6 - l^2x^5 + l^3x^4\right). \tag{37}$$

Consequently, the second-order moment of the deflection is

$$\mathbb{E}\left[Y^2(x)\right] = \sigma_Y^2(x) + \mathbb{E}[Y(x)]^2 = \frac{\lambda}{12}\mathbb{E}[F_i^2]\left(-\frac{2}{105}x^7 + \frac{1}{3}lx^6 - l^2x^5 + l^3x^4\right) + \frac{\lambda^2}{12}\mathbb{E}[F_i]^2\left(\frac{1}{48}x^8 - \frac{1}{6}lx^7 + \frac{7}{12}l^2x^6 - l^3x^5 + \frac{3}{4}l^4x^4\right). \tag{38}$$

This expression will be used later when applying the PME to approximate the 1-PDF of the deflection $Y(x)$.

Two characteristics that are very important when studying beams in engineering are the bending moment, $M(x)$, and the shear force, $T(x)$, defined as $M(x) := -EIY''(x)$ and $T(x) := -EIY'''(x)$, respectively [21]. These physical quantities can be calculated differentiating (20)–(6), and taking into account that, by (5), $R_3''(x) = R_1(x)$ and $R_3'''(x) = R_0(x)$, so $G_3''(x) = G_1(x)$ and $G_3'''(x) = G_0(x)$. Consequently,

$$M(x) = -G_1(x) + G_1(l) - G_0(l)(l - x), \tag{39}$$

and

$$T(x) = -G_0(x) + G_0(l). \tag{40}$$

Applying the expectation operator in (39) and (40), and using the expressions obtained in (24) and (25), one calculates the value of the mean of the bending moment

$$\mathbb{E}\left[M(x)\right] = -\frac{1}{2}\lambda\mathbb{E}\left[P_i\right]\left(x^2 + l^2 - 2lx\right), \tag{41}$$

and the shear force

$$\mathbb{E}\left[T(x)\right] = -\lambda\mathbb{E}\left[P_i\right](x - l). \tag{42}$$

Now, we compute the variance of the bending moment of the beam

$$\begin{aligned}\sigma_M^2(x) = C_M^{(2)}(x,x) &= \mathbb{E}\left[M(x)^2\right] - \mathbb{E}\left[M(x)\right]^2 \\ &= \sigma_{G_1}^2(x) - 2C_{G_1}^{(2)}(x,l) + 2C_{G_1G_0}^{(2)}(x,l)(l-x) + \sigma_{G_1}^2(l) \\ &\quad - 2C_{G_1G_0}^{(2)}(x,l)(l-x) + \sigma_{G_0}^2(l)(l-x)^2.\end{aligned} \tag{43}$$

In the above expression, note that $\sigma_{G_1}^2(x)$ can be calculated by (33) changing l by x and F_i by P_i, the term $\sigma_{G_0}^2(l)$ can be determined similarly to (35) changing F_i by P_i, and the rest of the terms can be expressed in an analogous manner using, respectively, (10) and (13),

$$C_{G_1}^{(2)}(x,l) = \lambda\mathbb{E}[P_i^2]\int_0^x R_1(x-\rho)R_1(l-\rho)d\rho = \lambda\mathbb{E}\left[P_i^2\right]\left(\frac{x^2l}{2} - \frac{x^3}{6}\right), \tag{44}$$

$$C_{G_1G_0}^{(2)}(x,l) = \lambda\mathbb{E}[P_i^2]\int_0^x R_1(x-\rho)R_0(l-\rho)d\rho = \frac{\lambda}{2}\mathbb{E}\left[P_i^2\right]x^2. \tag{45}$$

Substituting these expressions in (43) and simplifying, one gets

$$\sigma_M^2(x) = \lambda\mathbb{E}\left[P_i^2\right]\left(x^2l - l^2x + \frac{1}{3}l^3 - \frac{1}{3}x^3\right). \tag{46}$$

Consequently, the second-order statistic of the bending moment, which will be required later to approximate its PDF via the PME, is given by

$$\mathbb{E}\left[M^2(x)\right] = \lambda\mathbb{E}\left[P_i^2\right]\left(x^2l - l^2x + \frac{1}{3}l^3 - \frac{1}{3}x^3\right) + \frac{1}{4}\lambda^2\mathbb{E}\left[P_i\right]^2\left(x^2 + l^2 - 2lx\right)^2. \tag{47}$$

Now, we complete similar calculations for the shear force. Its variance is given by

$$\sigma_T^2(x) = C_T^{(2)}(x,x) = \mathbb{E}\left[T(x)^2\right] - \mathbb{E}\left[T(x)\right]^2 = \sigma_{G_0}^2(x) - 2C_{G_0}^{(2)}(x,l) + \sigma_{G_0}^2(l). \tag{48}$$

Carrying out computations in a similar fashion as before, one obtains

$$\sigma_T^2(x) = -\lambda\mathbb{E}\left[P_i^2\right](x - l). \tag{49}$$

The second-order moment is given by

$$\mathbb{E}\left[T^2(x)\right] = \lambda(x-l)\left(-\mathbb{E}\left[P_i^2\right] + \lambda\mathbb{E}\left[P_i\right]^2(x-l)\right). \tag{50}$$

4. Computational implementation

This section presents an algorithm that allows us to simulate the analytical development shown in the previous section computationally. The proposed algorithm is based on Monte Carlo. The method consists of a random and repeated sampling of the stochastic process of the load function, $Q(x)$, and of the random variables of the moment of inertia, I, and Young's modulus, E. The objective is to obtain a number of simulations that together provide statistical information on the PDF of the deflection, slope, bending moment, and shear parameters of the beam.

The procedure has been divided into the following steps: (1) first, the beam is discretized (2) then the stochastic process of the load function is simulated for each of the discretized points of the beam, (3) in a third step, the random variables of the moment of inertia and Young's modulus are sampled and (4) with the values obtained, the functions describing the behavior of the beam are evaluated, and (5) finally, the process is repeated until it is obtained a set of simulations which adequately represents the uncertainty of the behavior of the beam.

After the general description, we now give a detailed step-by-step description of the procedure.

Step 1: Beam discretization. Given the discrete nature of computer science, it is necessary to deal with the stochastic model in a discrete manner. The Poisson counting process has λx as expected value, where x represents the position in the axis of the beam. Although it is a discrete-continuous process, its simulation is discrete as long as, computationally, you can only evaluate it in a finite set of x. The discretization of the beam is important because the simulation involves assuming that there can only be charge points at the discretized positions and hence an adequate discretization plays a key role to obtain accurate results. The approximate solution of the model (in our case, the deflection of the beam) between spatial points can be linearly interpolated by knowing the approximations at the adjacent points. Since the solution does not necessarily be linear, the distance between points must be small enough so that the error of the approximation is acceptable for the application of the numerical results. Ideally, the beam should be discretized at as many points as possible. However, the computational cost increases proportionally to the number of points used in the discretization. An appropriate strategy to optimize the trade-off between accuracy and computational cost is to generate more points where the greatest uncertainty in the solution is sensed, which generally coincides with the points of greatest structural weakness. If this intuition is not predisposed, the ideal is to consider evenly distributed points.

Step 2: Simulation of the stochastic process.

1. $\forall\, i \in \{0, 1, \ldots, D_b\}$ determining a spatial position x_i on beam b (where D_b is the total number of discretized points):
   - 1.1. $\forall\, m \in \{0, 1, \ldots, C_b\}$, determining the number of load functions c_m to be applied in beam b (where C_b is the total number of loads functions) with intensity Q_c and frequency f_c,
     - 1.1.1. The number of charge points s_i^m, generated by the charge function c_m at point x_i is obtained sampling from a Poisson distribution with parameter $\lambda := f_c/D_b > 0$, representing the expected value of s_i^m.
     - 1.1.2. $\forall k \in \{0, 1, \ldots, s_i^m\}$, the value of the point charge P_i is:

$$P_i^k = P_i^{k-1} + Q_c, \tag{51}$$

where $P_i^{k-1} = 0$ if $k = 0$ and where in the case that is a random variable, it is necessary to sample a value of its PDF. The distribution of Q_c can

be any positive/negative and continuous/discrete random variable. It can even be a nonparametric distribution constructed from field data.

At the end of the different loops, a value of $P_i^{s_i^m}$ (hereafter P_i) will have been obtained for each x_i.

2. The next step is to obtain the value of the net charge function $G_j(x),\ j = 0, 1, 2, 3$.

2.1. $\forall\ i\ \in \{0, 1, \dots, D_b\}$:

2.1.1. $\forall\ z\ \in \{0, 1, \dots, D_b\}$:
If $x_i < x_z$:

$$G_0(x_i) = G_0(x_i) + 0, \tag{52}$$

$$G_1(x_i) = G_1(x_i) + 0, \tag{53}$$

$$G_2(x_i) = G_2(x_i) + 0, \tag{54}$$

$$G_3(x_i) = G_3(x_i) + 0. \tag{55}$$

If $x_i > x_z$:

$$G_0(x_i) = G_0(x_i) + P_i, \tag{56}$$

$$G_1(x_i) = G_1(x_i) + P_i(x_i - x_z), \tag{57}$$

$$G_2(x_i) = G_2(x_i) + \frac{1}{2}P_i(x_i - x_z)^2, \tag{58}$$

$$G_3(x_i) = G_3(x_i) + \frac{1}{3!}P_i(x_i - x_z)^3. \tag{59}$$

Step 3: Simulation of the random variables. The values of the inertial moment, I_b, and Young's modulus, E_b, are obtained by sampling from their corresponding PDFs. The distribution of these random variables can be any positive parametric one. It can even be a nonparametric distribution constructed from field data.

***Step 4: Evaluation of beam performance functions.*.** Once the deterministic values of all the variables have been obtained by simulation, we take advantage of the analytical development introduced in the previous section to determine the behavior of the beam with respect to its deflection (Eq. (20)) and, therefore, its moment of inertia (Eq. (39)) and shear force (Eq. (40)).

1. $\forall\ i\ \in \{0, 1, \dots, D_b\}$:

$$Y_b(x_i) = \frac{1}{E_b I_b}\left[G_3(x_i) - \frac{1}{6}G_0(l)x_i^3 - \frac{1}{2}\left(G_1(l) - lG_0(l)\right)x_i^2\right], \tag{60}$$

$$M_b(x_i) = -G_1(x_i) + G_1(l) - G_0(l)(l - x_i), \tag{61}$$

$$T_b(x_i) = -G_0(x_i) + G_0(l). \tag{62}$$

Step 5: Repeat steps 1–4 until it is obtained a set of simulations. Once all the Steps 1–4 have been simulated, the result of one simulation is obtained. To determine the distribution of deflection, bending moment, and shear force of the beam, it is necessary to perform multiple simulations by repeating Steps 1–4. The greater the number of simulations, N, the better results will be obtained from the statistical analysis.

Once a large set of simulations has been generated, it is possible to construct the 95%CI (confidence intervals):

$\forall\ i\ \in \{0, 1, \dots, D_b\}$:

$$95\%\text{CI of } Y_b(x_i) = \left(\mathbf{P}_{2.5}([Y_b^0, Y_b^1, \dots, Y_b^n]),\ \mathbf{P}_{97.5}([Y_b^0, Y_b^1, \dots, Y_b^n])\right), \tag{63}$$

Table 1
Comparison of the mean, $\mathbb{E}[Y(x)]$, and the variance, $\sigma_Y^2(x)$, of the static deflection of the cantilever beam at different spatial points $x \in \{0, 1, 2, \dots, 10\}$ using the theoretical approach (Eq. (28) and Eq. (37) for computing $\mathbb{E}[Y(x)]$ and $\sigma_Y^2(x)$, respectively), and 100.000 simulations via Monte Carlo.

x	$\mathbb{E}[Y(x)]$ (Eq. (28))	$\mathbb{E}[Y(x)]$ (simulation)	$\sigma_Y^2(x)$ (Eq. (37))	$\sigma_Y^2(x)$ (simulation)
0	0	0	0	0
1	0.000463	0.000463	$1.486249 \cdot 10^{-8}$	$1.563205 \cdot 10^{-8}$
2	0.001730	0.001731	$2.140720 \cdot 10^{-7}$	$2.248590 \cdot 10^{-7}$
3	0.003633	0.003634	$9.721975 \cdot 10^{-7}$	$1.019968 \cdot 10^{-6}$
4	0.006023	0.006025	$2.746732 \cdot 10^{-6}$	$2.878598 \cdot 10^{-6}$
5	0.008772	0.008773	$5.974110 \cdot 10^{-6}$	$6.254897 \cdot 10^{-6}$
6	0.011770	0.011770	$1.100046 \cdot 10^{-5}$	$1.150769 \cdot 10^{-5}$
7	0.014928	0.014928	$1.804558 \cdot 10^{-5}$	$1.886364 \cdot 10^{-5}$
8	0.018177	0.018175	$2.719839 \cdot 10^{-5}$	$2.841349 \cdot 10^{-5}$
9	0.021467	0.021464	$3.844254 \cdot 10^{-5}$	$4.013907 \cdot 10^{-5}$
10	0.024769	0.024730	$5.171033 \cdot 10^{-5}$	$5.382120 \cdot 10^{-5}$

$$95\%\text{CI of } M_b(x_i) = \left(\mathbf{P}_{2.5}([M_b^0, M_b^1, \dots, M_b^n]),\ \mathbf{P}_{97.5}([M_b^0, M_b^1, \dots, M_b^n])\right), \tag{64}$$

$$95\%\text{CI of } T_b(x_i) = \left(\mathbf{P}_{2.5}([T_b^0, T_b^1, \dots, T_b^n]),\ \mathbf{P}_{97.5}([T_b^0, T_b^1, \dots, T_b^n])\right), \tag{65}$$

where $n \in \{0, 1, \dots, N\}$ and $\mathbf{P}$ represents the percentile function.

5. Numerical example

This section is addressed to apply the theoretical findings established in the previous sections by means of a full illustrative example.

Let us consider a 10m long overhanging beam (cantilever) in form of a balcony or lookout made up of an IPE 450 steel profile whose moment of inertia, I, is 33740cm^4 ±2%, and whose Young's modulus, E, is 210Mpa [22]. Due to the heterogeneous properties of the steel, we will assume Young's modulus of the profile has some variability according to a Gaussian distribution with a mean of 210Mpa and a standard deviation of 5%. Just for illustrative purposes, let us assume the maximum capacity allowed in the lookout is 20 people. We will assume that each person weighs, on average, 700N (71.36 kg) with a standard deviation of 5%. The above description corresponds with the following deterministic data of our modeling problem: $l = 10$, and $\lambda = 20$. While for the random parameters, and according to the foregoing description, we will assume that the Young's modulus of elasticity, E, has a truncated Gaussian distribution, $E \sim \mathrm{N}_{\mathcal{T}}(210 \cdot 10^9; 0.05 \cdot 210 \cdot 10^9)\mathrm{N/m}^2$, where $\mathcal{T} = [209.9993 \cdot 10^9, 210.0006 \cdot 10^9]$. The moment of inertia, I, has a Gaussian distribution, $I \sim \mathrm{N}(33740 \cdot 10^{-8}; 0.02 \cdot 33740 \cdot 10^{-8})\mathrm{m}^4$. And, finally, let us assume that the intensity of the concentrated loads P_i follows a Gaussian distribution, $P_i \sim \mathrm{N}(700; 35)\mathrm{N}$. We consider that E, I and P_i are independent random variables.

In Table 1, we show a comparison of the mean and the variance of the static deflection, $Y(x)$, given by expression (28) and (37), respectively, and the mean and variance obtained by Monte Carlo simulation following the procedure described in Section 4. We can observe that the values are in full agreement.

Once we have obtained the mean, $\mathbb{E}[Y(x)]$, and the variance, $\sigma_Y^2(x)$, we use the PME to compute the 1-PDF of the static deflection, $f_{Y(x)}(y)$. As we have seen in Section 2.3, for each x, we first solve the system (17) for $\lambda_i = \lambda_i(x)$, $i = 0, 1, 2$. For example, for the free-end, $x = 10$, where the mean and variance of the deflection are maxima, the 1-PDF is given by

$$f_{Y(10)}(y) = \mathbb{1}_{\mathcal{D}(Y(10))}e^{-1+0.893356-477.134605y+9633.765685y^2}, \tag{66}$$

where we have taken as domain the interval $\mathcal{D}(Y(10)) = [0, 0.096694]$ is constructed using the Chebyshev–Bienaymé's inequality [23] with 10

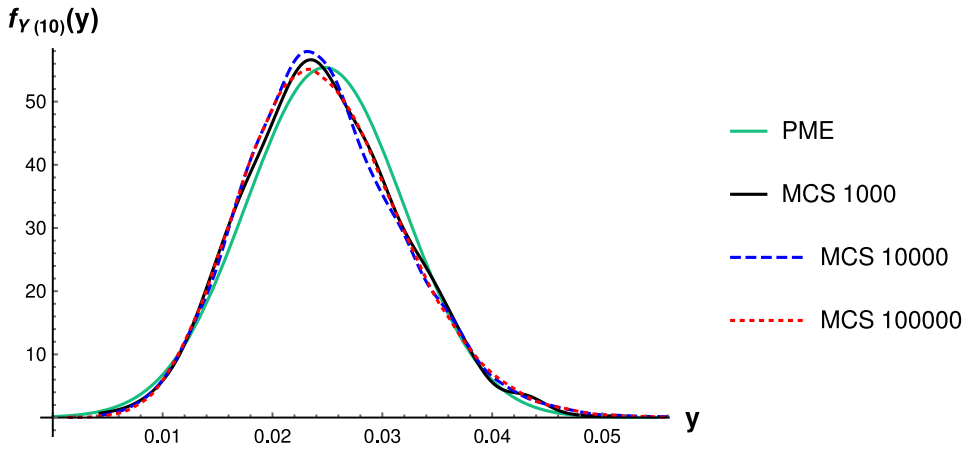

Fig. 2. 1-PDF of the static deflection of the cantilever beam, $f_{Y(x)}(y)$, at the spatial point $x = 10$ obtained via PME and Monte Carlo using 1000, 10,000 and 100,000 simulations.

Table 2
Comparison of the mean, $\mathbb{E}[M(x)]$, and the variance, $\sigma^2_M(x)$, of the bending moment of the cantilever beam at different spatial points $x \in \{0, 1, 2, \ldots, 10\}$ using the theoretical approach (Eq. (41) and Eq. (46) for computing $\mathbb{E}[M(x)]$ and $\sigma^2_M(x)$, respectively), and 100000 simulations via Monte Carlo.

x	$\mathbb{E}[M(x)]$ (Exp. (41))	$\mathbb{E}[M(x)]$ (simulation)	$\sigma^2_M(x)$ (Eq. (46))	$\sigma^2_M(x)$ (simulation)
0	−69993.699374	−69878.898675	$3.274244 \cdot 10^8$	$3.291509 \cdot 10^8$
1	−56694.896493	−56586.404173	$2.386924 \cdot 10^8$	$2.399465 \cdot 10^8$
2	−44795.967599	−44696.961390	$1.676413 \cdot 10^8$	$1.685314 \cdot 10^8$
3	−34296.912693	−34206.526813	$1.123065 \cdot 10^8$	$1.128808 \cdot 10^8$
4	−25197.731774	−25118.063711	$7.072368 \cdot 10^7$	$7.103806 \cdot 10^7$
5	−17498.424843	−17432.235020	$4.092805 \cdot 10^7$	$4.104798 \cdot 10^7$
6	−11198.991899	−11145.801799	$2.095516 \cdot 10^7$	$2.096393 \cdot 10^7$
7	−6299.432943	−6258.001079	$8.840460 \cdot 10^6$	$8.808880 \cdot 10^6$
8	−2799.747974	−2768.248438	$2.619395 \cdot 10^6$	$2.586399 \cdot 10^6$
9	−699.936993	−681.106878	$3.274244 \cdot 10^5$	$3.145759 \cdot 10^5$
10	0	0	0	0

Table 3
Comparison of the mean, $\mathbb{E}[T(x)]$, and the variance, $\sigma^2_T(x)$, of the shear force of the cantilever beam, at different spatial points $x \in \{0, 1, 2, \ldots, 10\}$ using the theoretical approach(Eq. (40) for $\mathbb{E}[T(x)]$ and Eq. (49) for $\sigma^2_T(x)$, respectively,), 100000 simulations via Monte Carlo.

x	$\mathbb{E}[T(x)]$ (Eq. (40))	$\mathbb{E}[T(x)]$ (simulation)	$\sigma^2_T(x)$ (Eq. (49))	$\sigma^2_T(x)$ (simulation)
0	13998.739874	13989.984660	$9.822734 \cdot 10^6$	$9.868522 \cdot 10^6$
1	12598.865887	12584.463060	$8.840460 \cdot 10^6$	$8.871837 \cdot 10^6$
2	11198.991899	11184.844909	$7.858187 \cdot 10^6$	$7.891253 \cdot 10^6$
3	9799.117912	9787.433546	$6.875913 \cdot 10^6$	$6.893854 \cdot 10^6$
4	8399.243924	8387.069932	$5.893640 \cdot 10^6$	$5.922317 \cdot 10^6$
5	6999.369937	6985.927374	$4.911367 \cdot 10^6$	$4.941940 \cdot 10^6$
6	5599.495949	5588.894615	$3.929093 \cdot 10^6$	$3.946902 \cdot 10^6$
7	4199.621962	4191.937526	$2.946820 \cdot 10^6$	$2.953221 \cdot 10^6$
8	2799.747974	2792.303398	$1.964546 \cdot 10^6$	$1.971305 \cdot 10^6$
9	1399.873987	1391.025322	$9.822734 \cdot 10^5$	$9.818576 \cdot 10^5$
10	0	0	0	0

standard deviations around the mean (and truncating the left-end of the interval to 0 value in order to keep consistent with the physical meaning of the deflection) so that $\int_{\mathcal{D}(Y(10))} f_{Y(10)}(y)dy \approx 1$. To better compare the results obtained using the PME against the ones calculated by Monte Carlo, in Fig. 2, we show the corresponding using Monte Carlo with simulations 1000, 10000, and 100,000 simulations at the spatial point, $x = 10$. Although we can observe a good agreement between them, it is worth to point out that this little discrepancy can be explained because when applying the PME we retain the information provided by the two first moments, then being Gaussian the approximation while the response could be non-Gaussian.

Now, we study the bending moment, $M(x)$. In Table 2, we compare the mean and the variance of $M(x)$, given by expression (41) and (46), respectively, and the ones computed by Monte Carlo using 100,000 simulations. We can observe, again, that the values show good agreement.

The 1-PDF of the bending moment, $f_{M(x)}(m)$, can also be computed by the PME. Its approximation at the spatial point $x = 0$, where its mean (in absolute value) and variance are maxima, is given by

$$f_{M(0)}(m) = \mathbb{1}_{\mathcal{D}(M(0))} e^{-1-17.197008-0.000213\ m-1.524656m^2}, \tag{67}$$

where, similarly as it was done for the deflection, the domain $\mathcal{D}(M(0)) = [-250931.572337, 0]$ has been calculated using the Chebyshev-Bienaymé's inequality with 10 standard deviations and taking into account that the bending moment is non-positive.

In Fig. 3, we show a graphical representation of the 1-PDF given by (67) and the ones obtained by Monte Carlo using 1000, 10,000, and 100,000 simulations. We can observe the results are fully consistent.

In Table 3, we compare the values obtained of the mean, $\mathbb{E}[T(x)]$, and the variance, $\sigma^2_T(x)$, of the shear force, $T(x)$, given by expression (42) and (49), respectively, and the ones computed by Monte Carlo using 100,000 simulations. Note that the results show good agreement.

As before, to complete the probabilistic analysis, we approximate the 1-PDF of the shear force, $f_{T(x)}(t)$, using the PME. It results

$$f_{T(0)}(t) = \mathbb{1}_{\mathcal{D}(T(0))} e^{-1-17.943337+0.001424t-5.088214\cdot 10^{-8}t^2}, \tag{68}$$

where $\mathcal{D}(T(0)) = [0, 45347.054670]$.

Finally, in Fig. 4 we compare the three approximations of 1-PDF obtained by Monte Carlo with 1000, 10,000 and 100,000 simulations against the one obtained by Eq. (68) at the spatial point $x = 0$. The results show a full agreement as the number of simulation increase.

Now, we are going to compare the theoretical and Monte Carlo approximations of the expectation of all the physical quantities studied for the cantilever, namely, the deflection, the bending moment and the shear force, using as goodness-of-fit the symmetric mean absolute percentage error (SMAPE). Let us recall that for a set of n theoretical values of the previous quantities, say Z_i and their corresponding approximations obtained by Monte Carlo, $\hat{z}_i$, the SMAPE is given by

$$\text{SMAPE} = \frac{100\%}{n} \sum_{i=1}^{n} \frac{|Z_i - \hat{z}_i|}{(|Z_i| + |\hat{z}_i|)/2}. \tag{69}$$

In Table 4, we show the SMAPE corresponding to the expectation of the deflection, $Y(x)$, the bending moment, $M(x)$, and the shear force, $T(x)$, at the spatial points $x = 0, 1, \ldots, 10$, considering the approximations obtained via Monte Carlo simulations (MCS) with a different number of samples (1000, 10,000 and 100,000). It must be noticed that we apply the SMAPE with $n = 10$ since we must exclude the term $x = 10$, in the case of the deflection, and $x = 0$, in the case of the bending moment and the shear force, since their values are zero. We can observe that

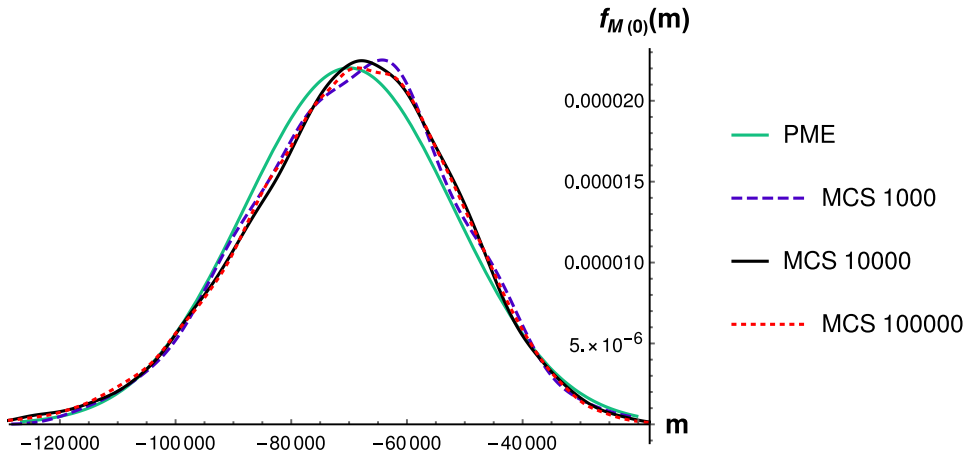

Fig. 3. 1-PDF of the bending moment of the cantilever beam, $f_{M(x)}(y)$, obtained via PME and Monte Carlo using 1000, 10,000, and 100,000 simulations at the spatial point $x = 0$.

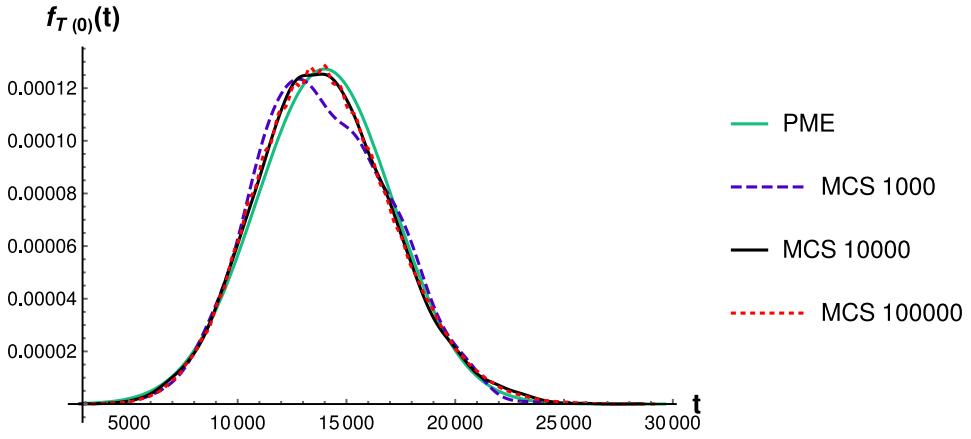

Fig. 4. 1-PDF of the shear force of the cantilever beam, $f_{T(x)}(t)$, at the spatial point $x = 0$ obtained via PME and Monte Carlo using 1000, 10,000 and 100,000 simulations.

Table 4
Computation of the SMAPE calculated by (69) of the theoretical expectation and the mean calculated via Monte Carlo simulations (MCS) with different samples (1000, 10000 and 100000) the deflection, bending moment, and shear force of the cantilever.

SMAPE (%)	1000 MCS	10000 MCS	MCS 100000
$Y(x)$	0.288816	0.245558	0.032886
$M(x)$	0.824381	1.004208	0.653084
$T(x)$	0.726415	0.442595	0.203296

the SMAPE is significantly reduced when using 100,000 simulations, as expected.

We finish this section by comparing the mean and confidence intervals of the deflection, bending moment, and shear force, which we have obtained theoretically and by simulations. First, we take advantage of the 1-PDF computed through PME to construct 95% confidence intervals. To do this for the deflection $Y(x)$ (similarly is done for the bending moment, $M(x)$, and the shear force, $T(x)$), we need to obtain $k(x)$ satisfying

$$\int_{\mathbb{E}[Y(x)]-k(x)\sigma_{Y(x)}}^{\mathbb{E}[Y(x)]+k(x)\sigma_{Y(x)}} f_{Y(x)}(y) = 0.95, \tag{70}$$

where $f_{Y(x)}(y)$ is the 1-PDF of the deflection. Second, from the Monte Carlo simulations, we obtain the confidence intervals using the algorithm based on the percentile function explained in Step 5 in Section 4.

In Fig. 5, we show the mean and confidence intervals of the deflection, $Y(x)$. We can observe that the results provided using both approaches are very close, showing better agreement in the case of the approximation of the mean $\mathbb{E}[Y(x)]$, as expected. Although the value of $k(x) := k_Y(x)$ obtained from (70) may change with the spatial position x, in this case, we have obtained $k_Y(x) \approx 1.96$ for all $x = 1, \ldots, 10$.

Analogously, in Figs. 6 and 7, we show the corresponding plots for the bending moment, $M(x)$, and the shear force, $T(x)$. Here, it is worth pointing out that the value of k changes as x does. In the case of the bending moment, $k(x) := k_M(x) \approx 1.96$ for $x \in \{0, \ldots, 6\}$, $k_M(7) \approx 1.9$, $k_M(8) \approx 1.75$, and $k_M(9) \approx 1.32$. While for the share force, $k_T(x) \approx 1.96$ for $x \in \{0, \ldots, 6\}$, $k_T(7) \approx 1.95$, $k_T(8) \approx 1.87$, and $k_T(9) \approx 1.51$.

To better understand the behavior indicated for $k = k(x)$ in each of the three cases, let us observe that we have approximated the corresponding 1-PDFs by applying the PME imposing three constraints (first, the one corresponding to the normalization condition and the others two corresponding to the two first statistical moments). In this manner, we determine a (truncated) Gaussian-like approximation. As can be seen in Fig. 8, the approximations for $f_{Y(x)}(y)$ are roughly symmetric for every spatial position x (in Fig. 8(a) we show the results including all values of x, and in Fig. 8(b) we zoom-up a few values so that the symmetry can be better graphically assessed). So, the classical Gaussian 2σ rule-of-thumb [23], corresponding to $k \approx 1.96$, is fulfilled. For the case of $f_{M(x)}(m)$, it can be seen that symmetry is roughly preserved for $x \in \{0, \ldots, 6\}$ and deteriorates thereafter (see Figs. 8(c)–8(d)). Consequently, the approximation of $f_{M(x)}(m)$ is no longer Gaussian, and the value of k departs from 1.96. An analogous explanation, can be given for the case of $f_{T(x)}(t)$ (see Figs. 8(e)–8(f)). In this latter case, it is worth pointing out that we can also observe that in the case of the calculation of the percentiles of $f_{T(x)}(t)$, there are steps in the functions. This is because the shear force is defined by a linear function of $G_0(x)$, see Eq. (62), which corresponds to the step function. The

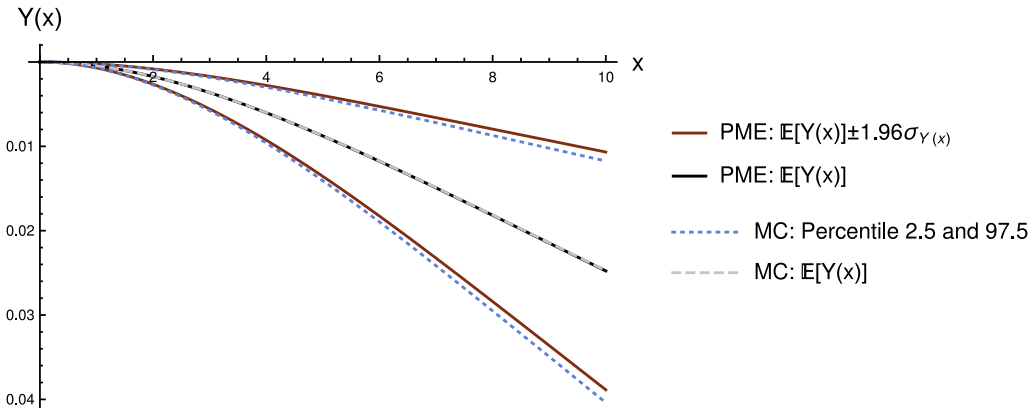

Fig. 5. Comparison of the mean and confidence intervals of the static deflection, $Y(x)$, using the PME and Monte Carlo simulations.

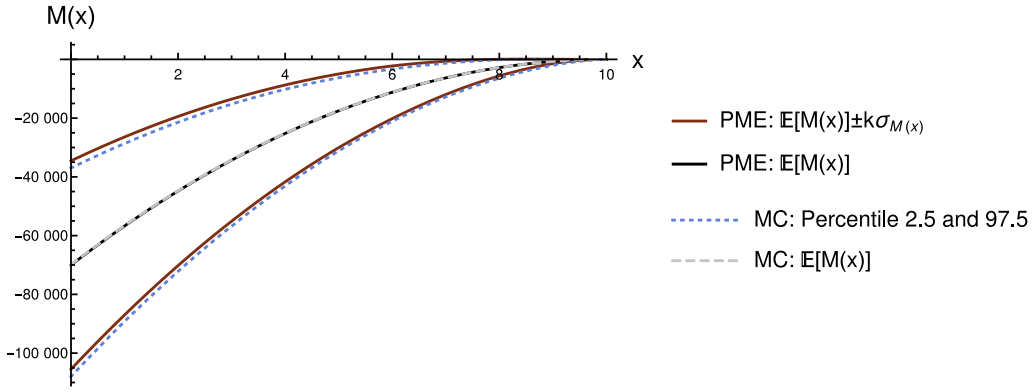

Fig. 6. Comparison of the mean and confidence intervals of the bending moment, $M(x)$, using the PME and Monte Carlo simulations.

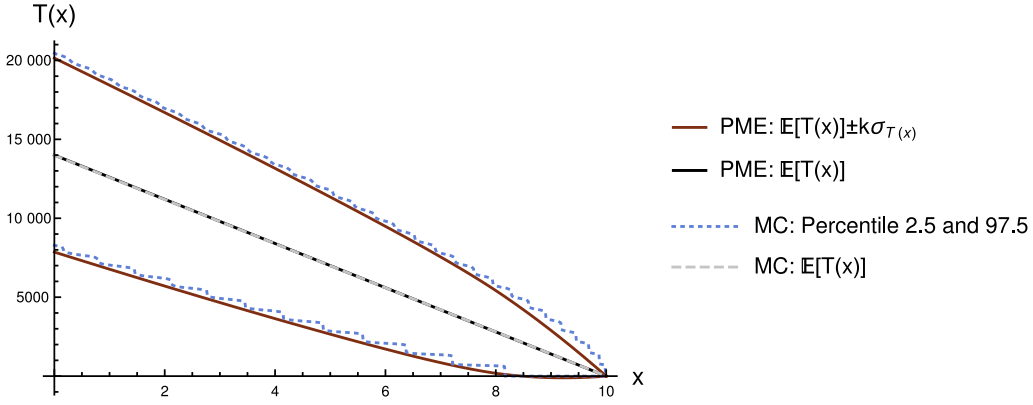

Fig. 7. Comparison of the mean and confidence intervals of the shear force, $T(x)$, using the PME and Monte Carlo simulations.

differences in the smoothness of the steps are due to the influence of the random intense load, P_i, in extreme cases. Simulating this parameter as a deterministic one, it has been observed that both functions reduce the smoothness of their steps. This verification has also been done with the parameters corresponding to the structural characteristics, E and I, observing that their variability has no impact on the smoothness of the steps.

6. Conclusions

In this paper, we have performed a full probabilistic analysis of a cantilever beam using the Euler–Bernoulli's theory. For the sake of generality, in our study, we have assumed that all the model parameters (the moment of inertia, I, and Young's modulus, E) are independent random variables with arbitrary density functions, and the load acting on the beam is described by means of the delta-correlated process. The adopted approach has made it possible the computation of the mean and the variance of the static deflection, the bending moment, and the shear force, with the purpose of later obtaining the first probability density function taking advantage of the Principle of Maximum Entropy. In the numerical example, we have compared these results with simulations obtained using a Monte Carlo-based algorithm, with good results.

Acronyms

PDF: Probability density function
1-PDF: First probability density function

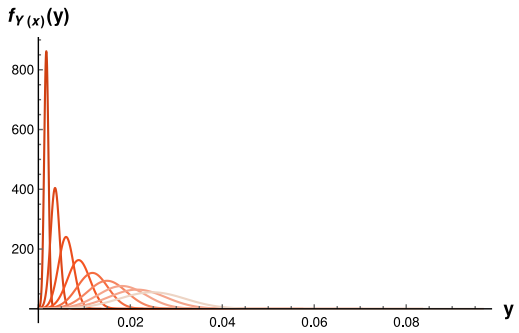

(a) 1-PDF of the deflection at the spatial points $x \in \{1, 2, 3, 4, 5, 6, 7, 8, 9\}$.

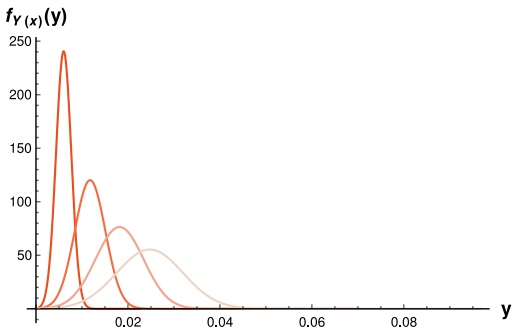

(b) 1-PDF of the deflection at the spatial points $x \in \{2, 4, 6, 8\}$.

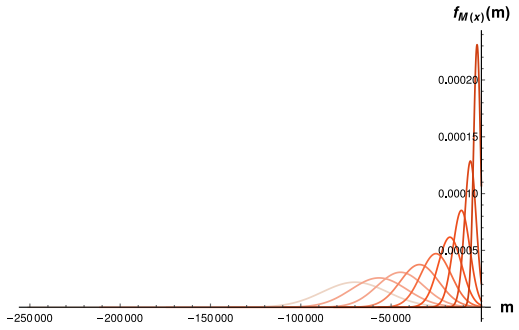

(c) 1-PDF of the bending moment at the spatial points $x \in \{0, 1, 2, 3, 4, 5, 6, 7, 8\}$.

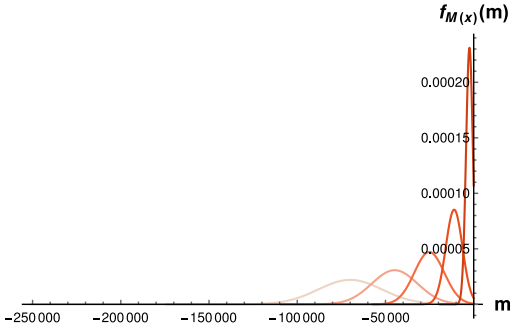

(d) 1-PDF of the bending moment at the spatial points $x \in \{0, 2, 4, 6, 8\}$.

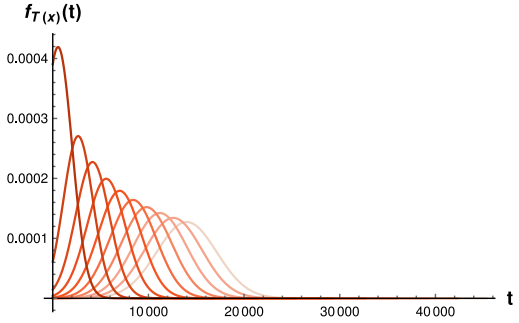

(e) 1-PDF of the shear force at the spatial points $x \in \{0, 1, 2, 3, 4, 5, 6, 7, 8, 9\}$.

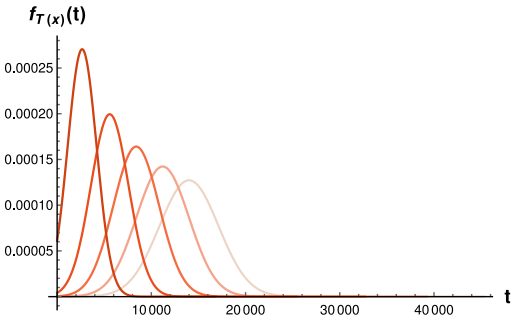

(f) 1-PDF of the shear force at the spatial points $x \in \{0, 2, 4, 6, 8\}$.

Fig. 8. 1-PDF of the different studied characteristics of the cantilever beam.

PME: Principle of Maximum Entropy
MCS: Monte Carlo simulations
SMAPE: Symmetric mean absolute percentage error

Declaration of competing interest

The authors declare the following financial interests/personal relationships which may be considered as potential competing interests: Juan Carlos Cortes reports financial support was provided by Agencia Estatal de Investgación. Maria Dolores Rosello reports financial support was provided by Generalitat Valenciana.

Data availability

No data was used for the research described in the article.

Acknowledgments

This work has been supported by the grant PID2020-115270GB–I00 funded by MCIN/AEI/10.13039/501100011033 and the grant AICO/2021/302 (Generalitat Valenciana). We give our deepest thanks to the two anonymous reviewers for their useful comments and suggestions that have improved the final version of the paper.

Appendix. Obtaining the solution of model (19)

The solution of model (1) is similar to the one obtained in [8], the difference lies in the type of beam, and therefore, in the boundary conditions of the model. Based on the solution

$$Y(x) = \frac{1}{EI}\sum_{i=1}^{N(l)} P_i R_3(x - x_i) + \frac{1}{6}C_1 x^3 + \frac{1}{2}C_2 x^2 + C_3 x + C_4, \tag{A.1}$$

we use the boundary conditions (2) in order to compute the integration constants C_1, C_2, C_3, and C_4.

First, we calculate C_4

$$Y(0) = 0 \rightarrow C_4 = 0, \tag{A.2}$$

and C_3

$$Y'(0) = 0 \rightarrow C_3 = 0, \tag{A.3}$$

Second, we calculate C_1 using the third derivative

$$Y'''(l) = 0 \rightarrow \frac{1}{EI}\sum_{i=1}^{N(l)} P_i R_0(l-x_i) + C_1 = 0 \rightarrow C_1 = -\frac{1}{EI}\sum_{i=1}^{N(l)} P_i R_0(l-x_i), \tag{A.4}$$

and finally, we calculate C_2

$$Y''(l) = 0 \rightarrow \frac{1}{EI}\sum_{i=1}^{N(l)} P_i R_1(l-x_i) - \frac{1}{EI}\sum_{i=1}^{N(l)} P_i R_0(l-x_i)l + C_2 = 0, \tag{A.5}$$

$$C_2 = -\frac{1}{EI}\left(\sum_{i=1}^{N(l)} P_i R_1(l-x_i) - \sum_{i=1}^{N(l)} P_i R_0(l-x_i)l\right). \tag{A.6}$$

Now, replacing the obtained integration constants into (A.1), using the Filtered Poisson Processes (6) and reorganizing the solution, one obtains

$$Y(x) = \frac{1}{EI}\left(G_3(x) - \frac{1}{6}G_0(l)x^3 - \frac{1}{2}\left(G_1(l) - lG_0(l)\right)x^2\right). \tag{A.7}$$

References

[1] A. Öchsner, Classical beam theories of structural mechanics, Springer International Publishing, 2021, http://dx.doi.org/10.1007/978-3-030-76035-9.

[2] R.A. Shetty, S.A. Deepak, K. Sudheer Kini, G.L. Dushyanthkumar, Bending deflection solutions of thick beams using a third-order simple single variable beam theory, in: K.K. Hau, A.K. Gupta, S. Chaudhary, T. Gupta (Eds.), Recent Advances in Structural Engineering and Construction Management, Springer Nature Singapore, Singapore, 2023, pp. 233–246.

[3] B. Biondi, S. Caddemi, Euler–Bernoulli beams with multiple singularities in the flexural stiffness, Eur. J. Mech. A Solids 26 (5) (2007) 789–809, http://dx.doi.org/10.1016/j.euromechsol.2006.12.005.

[4] J.A.M. Carrer, R.F. Scuciato, L.F.T. Garcia, The boundary element method applied to the analysis of Euler–Bernoulli and Timoshenko continuous beams, Iran. J. Sci. Technol. Trans. Civ. Eng. 44 (2020) 875–888, http://dx.doi.org/10.1007/s40996-020-00359-z.

[5] N. Malkiel, O. Rabinovitch, I. Elishakoff, Exact solutions for stochastic Bernoulli–Euler beams under deterministic loading, Acta Mech. 232 (6) (2021) 2201–2224, http://dx.doi.org/10.1007/s00707-020-02895-1.

[6] T.D. Hien, P.-C. Nguyen, Evaluation of response variability of Euler-Bernoulli beam resting on foundation due to randomness in elastic modulus, in: J.N. Reddy, C.M. Wang, V.H. Luong, A.T. Le (Eds.), ICSCEA 2019, Springer Singapore, Singapore, 2020, pp. 1087–1092.

[7] S. Pryse, S. Adhikari, Neumann enriched polynomial chaos approach for stochastic finite element problems, Probab. Eng. Mech. 66 (2021) 103157, http://dx.doi.org/10.1016/j.probengmech.2021.103157.

[8] G. Falsone, D. Settineri, Exact stochastic solution of beams subjected to delta-correlated loads, Struct. Eng. Mech. 47 (3) (2013) 307–329.

[9] R.-C. Hibbeler, Mechanics of Materials, Prentice Hall, 2008.

[10] G. Falsone, The use of generalised functions in the discontinuous beam bending differential equations, Int. J. Eng. Educ. 18 (3) (2002) 337–343.

[11] R.L. Stratonovich, Topics in the Theory of Random Noise, Gordon and Breach, New York, 1963.

[12] M. Grigoriu, Stochastic Calculus: Applications in Science and Engineering, Birkhauser, Boston, 2002.

[13] Y. Lin, Probabilistic Theory of Structural Dynamics, McGraw-Hill, 1967.

[14] J.V. Michalowicz, J.M. Nichols, F. Bucholtz, Handbook of Differential Entropy, CRC Press, Taylor & Francis Group, 2018.

[15] N.J. Yogalakshmi, K.B. Rao, Shear capacity distribution of reinforced concrete beams: An information theoretic entropy approach, Adv. Struct. Eng. 24 (15) (2021) 3452–3471, http://dx.doi.org/10.1177/13694332211029734.

[16] Q. Chen, H. Zhu, J. Ju, et al., A stochastic micromechanical model for fiber-reinforced concrete using maximum entropy principle, Acta Mech. 229 (2018) 2719–2735, http://dx.doi.org/10.1007/s00707-018-2135-1.

[17] J. Guo, J. Zhao, S. Zeng, Structural reliability analysis based on analytical maximum entropy method using polynomial chaos expansion, Struct. Multidiscip. Optim. 58 (2018) 1187–1203, http://dx.doi.org/10.1007/s00158-018-1961-z.

[18] X. Liu, X. Wang, J. Xie, B. Li, Construction of probability box model based on maximum entropy principle and corresponding hybrid reliability analysis approach, Struct. Multidiscip. Optim. 61 (2020) 599–617, http://dx.doi.org/10.1007/s00158-019-02382-9.

[19] M. Mazhdrakov, D. Benov, N. Valkanov, The Monte Carlo Method. Engineering Applications, ACMO Academic Press, Sofia, 2018.

[20] D. Xiu, Numerical Methods for Stochastic Computations: A Spectral Method Approach, Princeton University Press, Princeton, 2010.

[21] E.N. Strømmen, Structural Mechanics, Springer International Publishing, 2020, http://dx.doi.org/10.1007/978-3-030-44318-4.

[22] ASM Handbook Committee, Properties and Selection: Irons, Steels, and High-Performance Alloys, ASM International, 1990, http://dx.doi.org/10.31399/asm.hb.v01.9781627081610.

[23] G. Casella, R. Berger, Statistical Inference, second ed., Cengage Learning India, 2007.